Graphical Abstract

Understanding the effect of moderate concentration SDS on CO_2 hydrates growth in the presence of THF

Xinrui Cai, Joshua Worley, Anh Phan, Matteo Salvalaglio, Carolyn Koh, Alberto Striolo

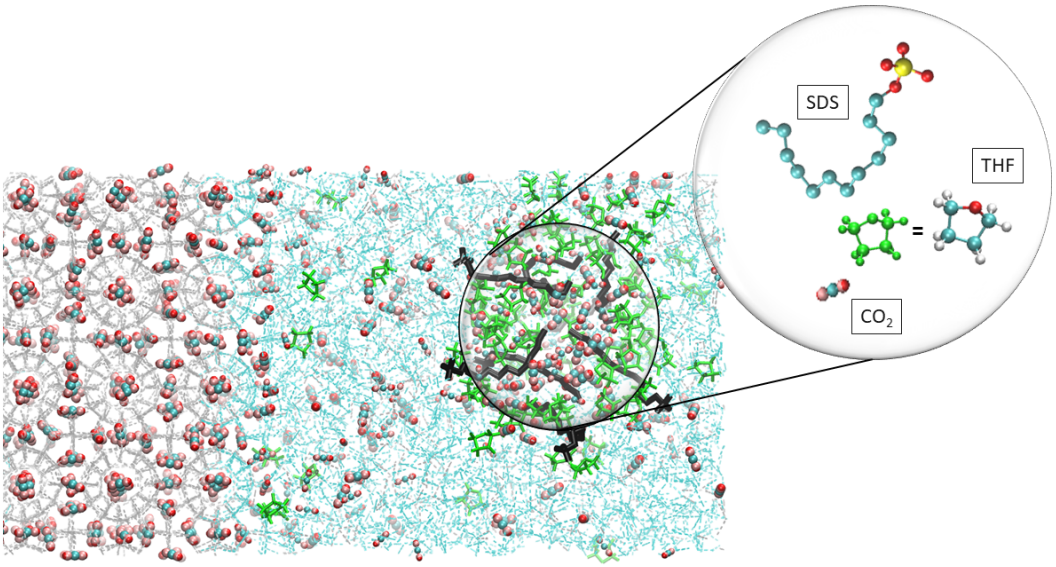

Highlights

Understanding the effect of moderate concentration SDS on CO_2 hydrates growth in the presence of THF

Xinrui Cai, Joshua Worley, Anh Phan, Matteo Salvalaglio, Carolyn Koh, Alberto Striolo

- SDS and THF prmoters are antagonistic when above a temperature threshold
- In the presence of THF and CO_2, SDS forms micellar aggregates
- Experiments support the simulation insights

Understanding the effect of moderate concentration SDS on CO_2 hydrates growth in the presence of THF

Xinrui Cai[a], Joshua Worley[b], Anh Phan[c], Matteo Salvalaglio[a], Carolyn Koh[b], Alberto Striolo[a,d]

[a] *Thomas Young Centre and Department of Chemical Engineering, University College London, Torrington Place, London, WC1E 7JE, United Kingdom*

[b] *Department of Chemical and Biological Engineering, Colorado School of Mines, Golden, CO 80401, United States*

[c] *School of Chemistry and Chemical Engineering, Faculty of Engineering and Physical Sciences,, University of Surrey, Guildford, Surrey GU2 7XH, United Kingdom*

[d] *School of Sustainable Chemical, Biological and Materials Engineering, University of Oklahoma, Norman, SOK 73019, United States*

Abstract

Hypothesis

Additives like Tetrahydrofuran (THF) and Sodium Dodecyl Sulfate (SDS) improve CO_2 hydrates thermal stability and growth rate when used separately. It has been hypothesised that combining them could improve the kinetics of growth and the thermodynamic stability of CO_2 hydrates.

Simulations and Experiments

We exploit atomistic molecular dynamics simulation to investigate the combined impact of THF and SDS under different temperatures and concentrations. The simulation insights are verified experimentally using pendant drop tensiometry conducted at ambient pressures and high-pressure differential scanning calorimetry.

Findings

Our simulations revealed that the combination of both additives is synergistic at low temperatures but antagonistic at temperatures above 274.1 K due to the aggregation SDS molecules induced by THF molecules. These aggregates effectively remove THF and CO_2 from the hydrate-liquid interface, thereby reducing the driving force for hydrates growth. Experiments revealed that the critical micelle concentration of SDS in water decreases by 20% upon the addition of THF. Further experiments showed that only small amounts of SDS with THF is sufficient to increase the CO_2 storage efficiency by over 40% compared to results obtained without promoters. These results provide microscopic insights into the mechanisms of THF and SDS promoters on CO_2 hydrates, which allow for determining the optimal condition for hydrate growth.

Keywords: Hydrates, Promoters, CO_2, SDS

1. Introduction

Clathrate hydrates are crystalline compounds. They comprise water molecules that are hydrogen-bonded to each other and guest molecules held by weak Van der Waals

forces [1]. There are commonly three types of hydrate structures, namely sI, sII and sH [2]. sI is the most predominant hydrate structure on earth and contains small molecules such as CO_2, and methane [3]. Larger molecules such as Tetrahydrofuran (THF) occupy larger cages and lead to the formation of sII hydrates instead [4]. These compounds (sII hydrates) are commonly found under anthropogenic environments [3].

Recent studies reported that CO_2 hydrates display great potential in carbon capture [5], storage [6] and sequestration [7] due to their stability at mild operating conditions at which they can achieve relatively high gas storage [8, 9]. The main obstacle for these hydrate-based technologies are slow formation rate and low thermal stability at ambient conditions [10].

CO_2 hydrate formation, growth and stability can be modulated using chemical additives. These additives can be classified into thermodynamic and kinetic promoters. Thermodynamic promoters such as THF and tetrabutylammonium bromide (TBAB) shift the melting conditions of hydrates to milder operating conditions (higher temperature and/or lower pressure) [11, 12]. On the other hand, kinetic promoters, usually surface active materials such as Sodium DodecylSulfate (SDS) or amino acids, accelerate hydrate growth[13, 14, 15].

While promoters can enhance the formation and stability of CO_2 hydrates, they can also have negative impacts. One major drawback is that they may lead to the formation of mixed hydrates leading to lower CO_2 occupancy since the hydrate cages may be occupied by the promoters instead. For example, it has been proven experimentally that THF occupies the large cavity of sII cages hence lowering CO_2 gas uptake, especially when the THF concentration is higher than 5.56% mol [16]. However, Phan et al. [17] identified a range of temperature and pressure conditions at which CO_2 hydrates can grow in the presence of small amounts of THF, achieving fast growth rate without compromising CO_2 storage capacity. Several experiments reported an optimal concentration for promoters, and it has been noted that adding more or fewer promoters reduces their performance[18, 19, 20]. It has also been observed that SDS alters the surface morphoogy of hydrates. When SDS is present, hydrates exhibit upward growth above the gas-liquid interface. When SDS is present, hydrates exhibit upward growth beyond the gas-liquid interface. In contrast, in systems without SDS, hydrates tend to grow downward, consequently impeding the process of mass transfer [21, 22]. Liang et al. observed that lumps of xenon hydrates formed at low SDS concentration, whereas a centric layer of hydrates formed at the gas-liquid interface at high concentration [22].

Few studies investigated the interactions between thermodynamic and kinetic promoters on hydrate growth. For example, Torre et al. [23] reported that the combination of thermodynamic (THF) and kinetic (SDS) promoters enhances the kinetics of CO_2 hydrates better than when only a single promoter is used. Veluswamy et al. [13] also discovered that combining low concentrations of THF and SDS in an unstirred system dramatically improves the gas uptake of CO_2 hydrates. Yet such synergistic effect only occurs under specific conditions. For instance, Wang et al. indicated that 2 mol% THF with 0.1 wt% SDS under stirring could improve hydrate formation by 12.7% as compared to growth from a pure THF solution. However, at a higher SDS concentration of 0.2 wt%, the improvement drops to 11.7% [24].

In recent years, computer simulations have gained wide popularity as they offer a cost-effective and efficient way to predict thermodynamic and kinetic properties. By simulating the complex molecular interactions between water, CO_2 and promoters,

computational simulations provide insights into the fundamental mechanisms that govern the stability and growth of the hydrates. Furthermore, computational simulations can provide a level of detail that is difficult to achieve through experimental methods alone. For instance, Phan et al. [17] recently proved, using the direct coexistence method, that THF shifts the equilibrium curve of CO_2 hydrates and facilitates CO_2 diffusivity into hydrate cages [17]. Several groups also used Monte Carlo simulations to investigate the growth of gas hydrates[25, 26]. These simulation studies achieved remarkable levels of agreement with experiments while elucidating molecular phenomena that were previously only hypothesised.

Within this landscape, we utilised atomistic MD simulation to understand hydrate growth in the presence of promoters at the molecular level. By simulating CO_2 hydrates at different temperatures and promoter concentrations, we aim to decipher the microscopic mechanism that allows THF and SDS to promote or inhibit hydrate growth. The remainder of the manuscript is organised as follows: we first introduce the simulation methodology and report a few details concerning the experimental techniques used to validate our predictions. We then discuss our results, starting from the computing simulations and continuing with the experimental validation ones. We conclude by generalising our results within the context of hydrates application in CO_2 capture, transport, and storage.

2. Methodology

2.1. Methodology

2.1.1. Simulation Setup

The initial configuration of the simulation box is set up as shown in Figure 1, where the hydrate phase is sandwiched by the bulk liquid phase along the z-direction. The hydrate slab, 4.812nm $\times$ 4.812nm $\times$ 4.812nm in dimension, is constructed using sI CO_2 hydrate cages as it is the most stable structure under our simulation conditions [27]. The structure of the hydrate cages was built based on the work of Takeuchi [28]. In addition to the 6948 water molecules, 240 CO_2 molecules, 8 SDS molecules and different amounts of THF (0/50/100) molecules were inserted into the bulk liquid phase. The concentration of THF in the bulk would thus range from 0mol% to 1.37mol%, which is expected to stabilise hydrates growth [29]. Periodic boundary conditions are applied in all directions. This renders the hydrate slab infinite in the XY direction, presenting two flat interfaces to the liquid phase perpendicular to the Z direction.

2.1.2. Molecular Models and Force Fields

We used the TIP4P/Ice model to describe water molecules as it has been shown that this water model reproduces results that are within a variation of 5K with the experimental values [30, 31]. Conde et al. compared the three-phase coexistence curve for methane hydrates using TIP4P, TIP4P/2005 and TIP4P/Ice water model [32]. The coexistence temperature obtained using the TIP4P/Ice model agrees best with experimental results, with only a 5K difference. Miguez et al. also compared the three-phase coexistence of CO_2 hydrates. TIP4P/Ice model predicts a melting point only 2K away from the experiment value [31]. The EPM2 [33] force field was used to model CO_2 molecules as several studies have shown its capability to predict CO_2 hydrates growth and dissociation [34, 31]. The general AMBER force field [35] was used for THF modelling due to its prior success in THF hydrate simulations [17].

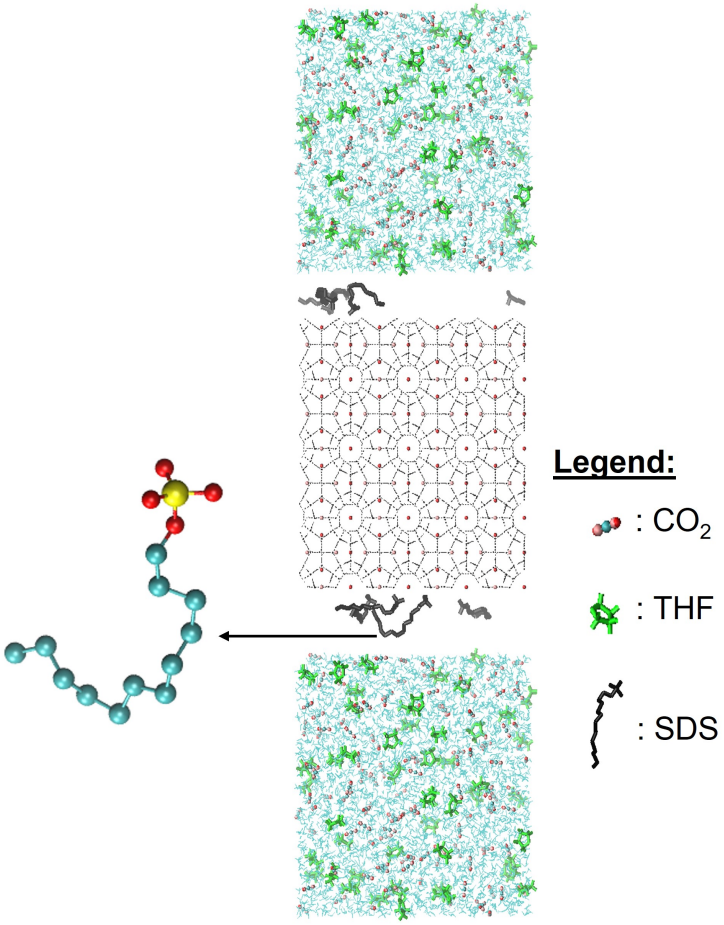

Figure 1: Snapshot of the initial configuration used for simulation. The cyan and grey lines represent water from the hydrate and liquid phases, respectively. Black molecules are SDS, green molecules are THF and cyan and red spheres are carbon and oxygen atoms, respectively, that together form CO_2. The chemical structure of SDS is shown on the left, where the cyan, red and yellow spheres represent Carbon, Oxygen and Sulfur atoms, respectively.

SDS molecules use the TraPPE force field for its hydrocarbon branch [31] and the Berkowitz model for the headgroup due to the presence of sulfonate [36]. Non-bonded interactions are modelled using electrostatic and dispersion forces. We used Coulomb interaction for electrostatic forces with a cut-off at 1.4nm, and the particle mesh Ewald method was chosen for long-range adjustment. Lennard-Jones interactions were also used for dispersion modelling at a cut-off of 1.4nm. Lorentz-Berthelot combining rules were used to estimate the LJ interactions for dissimilar atoms.

Numerous studies have substantiated the reliability of these forcefields[31, 32, 34]. For instance, Phan et al. [17] utilised TIP4P/ice, EPM2 and general AMBER forcefields to simulate CO_2 hydrates. Under these forcefields, the hydrates grow at 269.1K and 274.1K but initiate dissociation at a temperature of 279.1K. Remarkably, the dissociation temperature conforms to experimental observations.

2.1.3. Algorithm

We employed the direct coexistence method to simulate the growth and dissociation of CO_2 hydrates where the solid hydrate phase is in direct contact with the bulk liquid phase [37]. We describe the systems with atomistic resolution and integrate the equations of motion using the software package GROMACS 2021 [38]. The leapfrog algorithm is used to solve the equation of motion with a 1 fs timestep. Once the

initial configuration is prepared (see Figure 1), our protocol initiates with an energy minimisation via the steepest decent method. The system is simulated under NPT condition for 5ns to equilibrate the pressure utilising Berendsen pressure coupling [39]. Finally, 600ns NPT simulation was performed using Nosé-Hoover thermostat [40] and Parrinello-Rahman barostat [41]. The temperature and pressure were coupled at a time step of 0.5 ps. This ensures the rapid removal of latent heat released to the system by the phase transition [42]. The melting temperature of CO_2 hydrates at a pressure of 25.5 bar is experimentally determined to be 279.1K [43]. Our system is simulated at 269.1K, 274.1K, 279.1K and 284.1K and a pressure of 25.5 bar to favour hydrate growth. We extracted the configuration at every 50ns interval as the input and simulated it for a production phase of 1ns used for analysis.

2.1.4. Thickness Analysis

The growth and dissociation of the hydrate slab are calculated by quantifying its thickness as a function of simulation time. Whether water molecules are organised within the crystalline hydrate or are instead disordered in a liquid film is determined by quantifying the F4 order parameter using equation 1 [44] at every 50 ns

$$F4 = \frac{1}{k}\sum_{1}^{k} cos3\phi \tag{1}$$

In equation 1, ϕ refers to the H-O ... O-H torsional angle and k refers to the number of H-O...O-H bond pairs with bond length < 0.35nm. The F4 value for water molecules embedded in a hydrate environment is approximately 0.7, while that for water molecules in the liquid phase is close to 0 [45, 46]. This difference allows us to distinguish between hydrate and liquid phases, as illustrated in Figure 2. The region between the bulk liquid and hydrate is the interfacial transition region where partial hydrate cages are formed. The hydrate thickness is attained by measuring the width of the region when F4 > 0.3. The F4 value is computed from 1 ns simulations initiated from structures extracted at 50 ns intervals. Each of the 1 ns simulations is repeated 5 times by running MD simulations in series with the same initial configuration to attain an error bar associated with hydrate thickness.

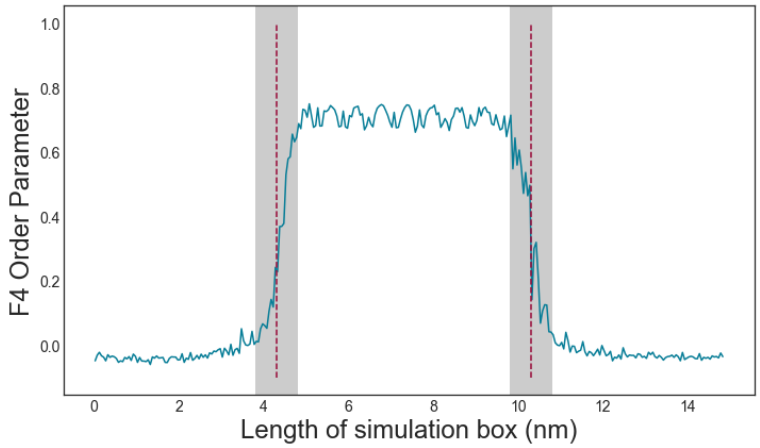

Figure 2: Example of F4 Order Parameter Profile along the simulation box at T=269.1K at 600ns. The dashed lines represent the locations when F4 reached 0.3 and the shaded region represents the hydrate-liquid interfacial region.

2.1.5. Clustering Analysis

An algorithm was implemented using PLUMED to identify and analyse the largest cluster of SDS molecules in solution. To this aim, we exploit the contact matrix to define a graph of connected SDS molecules and then determine the largest SDS cluster as the largest connected component of the graph[47, 48]. This is done by computing the distance between the centre of mass of each SDS molecule and defining them as bonded when the distance between their centres of mass is <0.8nm. Once the molecules belonging to the largest cluster are identified, we compute the centre of mass of the cluster and its diameter. CO_2 and THF molecules are considered trapped in the SDS cluster when found within the identified cluster radius. This procedure allows us to obtain aggregate size, aggregation number, and composition within an aggregate.

2.1.6. Experimental - Pendant Drop Tensiometry

An ambient condition pendant drop tensiometer (KSV instruments) was utilised to determine the critical micelle concentration (CMC) of SDS and SDS-THF solutions. A sketch of the experimental set-up is presented in Figure 3. CO_2 saturated de-ionised (DI) water was first prepared by bubbling CO_2 through a beaker of DI water for 12 hours. SDS solutions were then prepared from 0.001M to 0.015M by dissolving SDS into the CO_2 saturated water. These solutions were allowed 24 hours to reach equilibrium. The entire series was tested in the IFT apparatus using the pendant drop technique with the drop suspended in an open cuvette and monitored for 5 mins for each concentration tested. A total of 3 drops were tested for each concentration to produce an average surface tension value. The surface tension (ST) of each solution was calculated by solving the Young-Laplace equations for each droplet and plotted against the log of concentration to determine the switchover from the concentration-dependent ST region to the concentration-independent region. A similar methodology is used to obtain the ST of SDS in a SDS-THF-CO_2 solution. 0.476M of THF was added to SDS solutions ranging from 0.001M to 0.038M SDS, and ST was tested after a 5 min equilibration period which would minimise THF evaporation but still allow equilibrium to be reached.

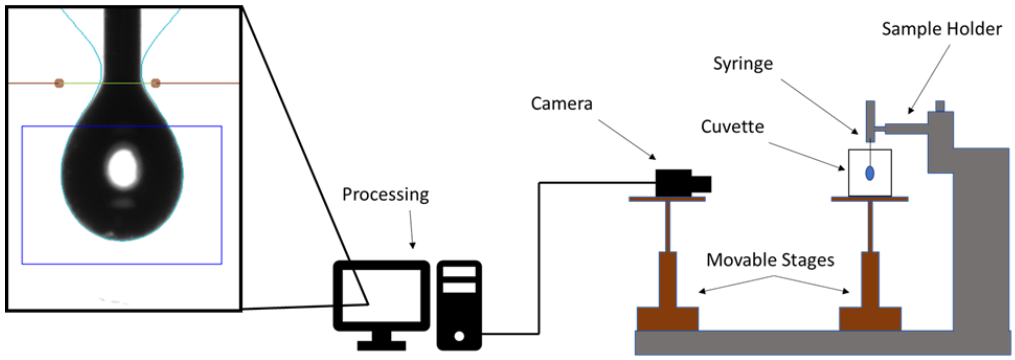

Figure 3: Schematich of pendant drop tensiometer utilised for IFT measurements

2.1.7. Experimental - High-Pressure Differential Scanning Calorimetry (HP-DSC)

A high pressure, low temperature Differential Scanning Calorimetry (HP-DSC) apparatus (Setaram microDSC VIIa) was utilised for hydrate growth testing as illustrated in Figure 4. Pure CO_2 hydrates and CO_2 hydrates formed with a combination of

THF + SDS were examined to determine the effect of the combination of promoters on hydrate growth and CO_2 uptake.

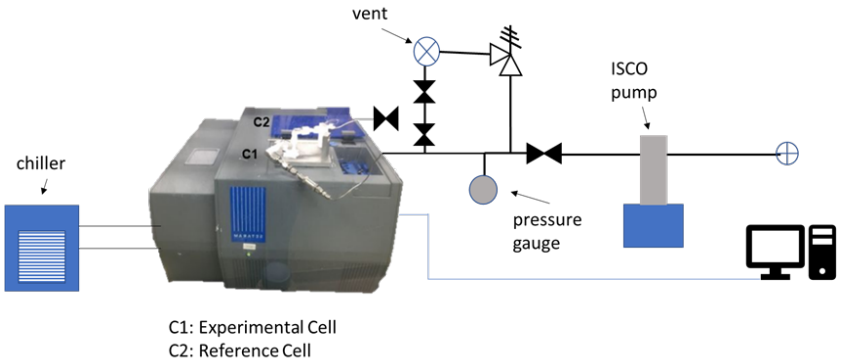

Figure 4: Schematic of the HPDSC apparatus used for this study

For the pure CO_2 hydrate experiments, approximately 15mg of DI water was added to the DSC cell, which was then sealed and placed into the apparatus. The cell was pressurized to 25.5 bar using CO_2 gas (99.998%, General Air). The sample was cooled to 253.15K and then heated to 293.15K at a rate of 1K/min for the first cycle to form ice and hydrate and induce the memory effect, then three repeat experiments were performed with the same limits and a cooling rate of 0.2K/min to allow measurement of heat release during dissociation.

For the CO_2-SDS tests, the same procedure was followed except that 0.001M and 0.038M solutions of SDS (>99.0%, Sigma Aldrich) in DI water were loaded into the cell. For the tests that involved the usage of THF, 10wt% solutions of THF (>99.9%, Sigma Aldrich) and DI water were loaded into the cell along with different concentrations of SDS solutions if needed. In these THF-related tests, the lower temperature limit was also increased to 263.15K to maintain the same subcooling as for the CO_2 and CO_2-SDS tests. All other parameters were the same. Conversions for CO_2 containing hydrates from each test were calculated in the same manner as [49] utilising the constants in Table 1.

-	Heat of Formation (kJ/mol)	Hydration Number	Reference
CO_2 Hydrate	70.8	5.9	[29, 50]
CO_2-10wt% THF	126.2[1]	20	[29, 51]

Table 1: Heat of formation and hydration number for CO_2 and CO_2-THF hydrate

For these conversion calculations, all hydrates containing THF and CO_2 were assumed to have a heat of dissociation similar to the 10wt% THF system. In cases where multiple peaks were discerned, the peaks were first identified and separated by the onset temperature and peak maximum temperature to determine which phase was likely present (CO_2 or CO_2-THF hydrate) and utilise the heat of dissociation corresponding to that phase. Subsequently, the conversion was computed for each isolated peak, and the resulting values were summed up to determine the overall total conversion.

[1]There is a wide spread in heat of formation predictions for THF-CO_2 hydrates. This value was selected as it was calculated at nearly identical conditions to the present studies

3. Results and Discussions

3.1. Simulated Hydrate Growth/Dissociation

Figure 5 presents the simulation results obtained for the hydrate growth profile at all temperatures and THF concentrations considered. The trend line for the growth profile is computed using logistic regression via Python's sklearn linear regression library. As seen in Figure 5, the hydrates grow or dissociate quickly within the initial 100ns and reach a plateau after that. This is due to the change in the composition of CO_2 in the bulk liquid, which alters the concentration driving force for hydrates growth/dissociation.

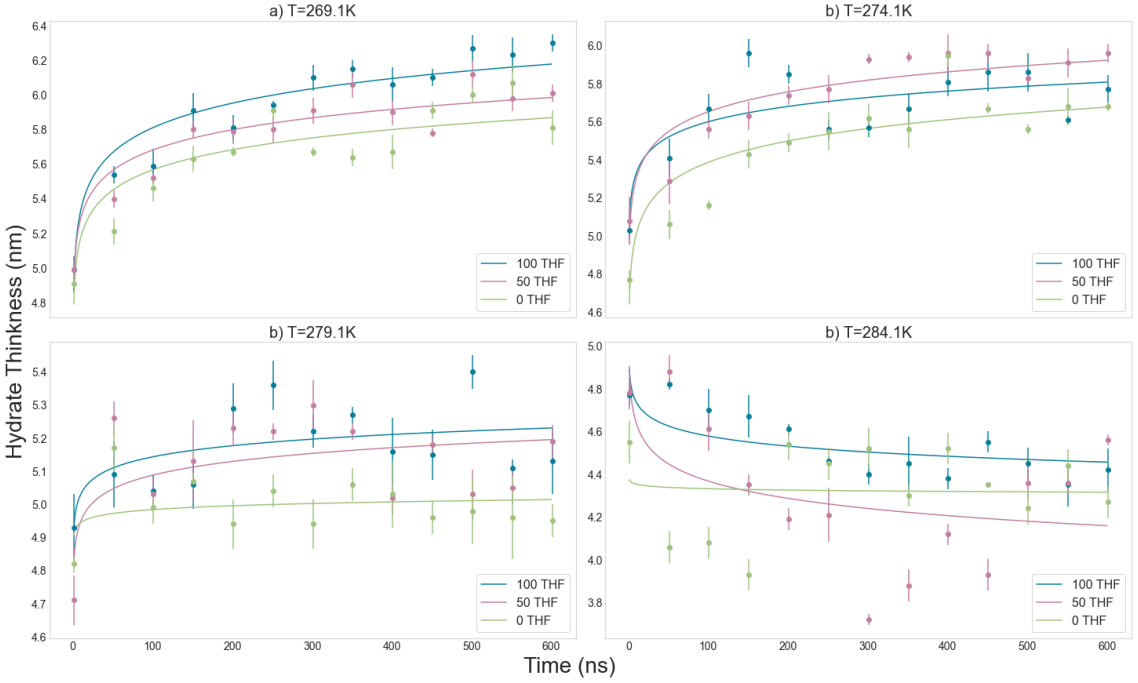

Figure 5: Comparison of hydrate thickness evolution over time with 0/50/100 THF molecules in the system at a) T=269.1K, b) T=274.1K, c) T=279.1K and d) T=284.1K

From the analysis of the growth profile, we observed that hydrates grow when T < 279.1 K. The melting temperature for systems without a thermodynamic promoter (THF) can be inferred as 279.1K, as the hydrate thickness stays roughly constant during our simulations at this temperature. This agrees well with experimental results where the melting temperature is determined to be around 279.1K [43]. For the systems with THF present at T = 279.1K, there is a minor growth at the beginning, but the thickness soon reaches a plateau. The plateau could be due to the reduction in driving force as CO_2 forms hydrates or the formation of micelle-like aggregates that will be discussed further in section 3.3. Above 279.1K, our results show signs of hydrate dissociation, which conform with experiments [52, 43]. Noticeably, the logistic regression fits the growth profile well at low temperatures. As temperature increases beyond 279.1K, the hydrate growth becomes unstable, and the logistic regression model under fits the simulation data, especially when no THF is present. This behaviour is expected, as experiments have shown that the hydrate structure fluctuates between dissociation and formation at moderately high temperatures[53]. In this study, we focus on hydrate growth at low temperatures, where logistic regression is effective in describing hydrate growth. We first discuss the results obtained in the presence of SDS.

3.2. Aggregate Formation

Visual analysis of the simulation trajectories reveals that the SDS molecules aggregate at high temperatures (T $\geq$ 274.1K). To further analyse the aggregation content, we plot the component concentration profile at the end of each simulation, i.e. at 600 ns.

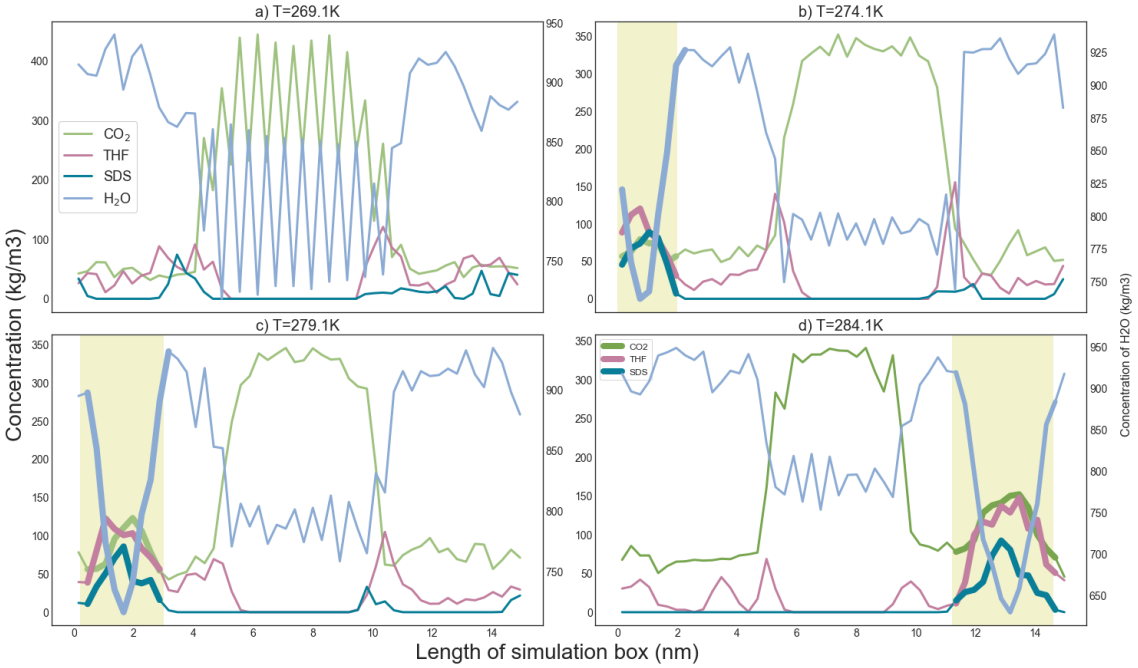

Figure 6: Concentration profile of CO_2, THF and SDS molecules within the simulation box with 100 THF molecules at a) T=269.1K, b)T=274.1K, c)T=279.1K, d)T=284.1K. The highlighted regions indicate the position of the aggregate containing SDS, THF and CO_2

There is no discernible concentration peak at T=269.1K as illustrated in Figure 6 (a), which reinforced that no aggregation occurred at this temperature. The lines from Figure 6 (b) are translated to the right along the x-axis by 0.25nm for a clearer identification of the aggregation cluster. In Figure 6 (b), (c) and (d), the SDS concentration peaks shown in the bulk liquid phase indicate the position of the aggregation. The alignment of THF and CO_2 concentration peaks with the SDS aggregation indicates that the aggregation also contains CO_2 and THF molecules. This is confirmed by visual analysis of the simulation snapshots. There is also a significant reduction of H_2O within the aggregates, which indicates that a hydrophobic environment would have formed. A closer look at the simulation snapshots using the software VMD (Figure 7) confirmed that the SDS hydrophobic tails always point towards the centre of the aggregates. In contrast, the hydrophilic head groups face towards the aqueous system. Such characteristics suggest that the SDS molecules within the system have indeed formed a micelle-like structure.

Such aggregates are roughly spherical in shape, which is typical of an SDS micelle in water at low concentration [54]. However, SDS micelles in water at ambient conditions are usually between 3.5 to 4 nm in size, which is larger than the aggregate obtained within our system, which is only 2.5 nm. Furthermore, the largest aggregate observed in our system at T = 284.1 K only has an aggregation number of 8 SDS molecules. This value is significantly smaller than a typical SDS micelle in water which is usually 30 at moderate SDS concentrations [55].

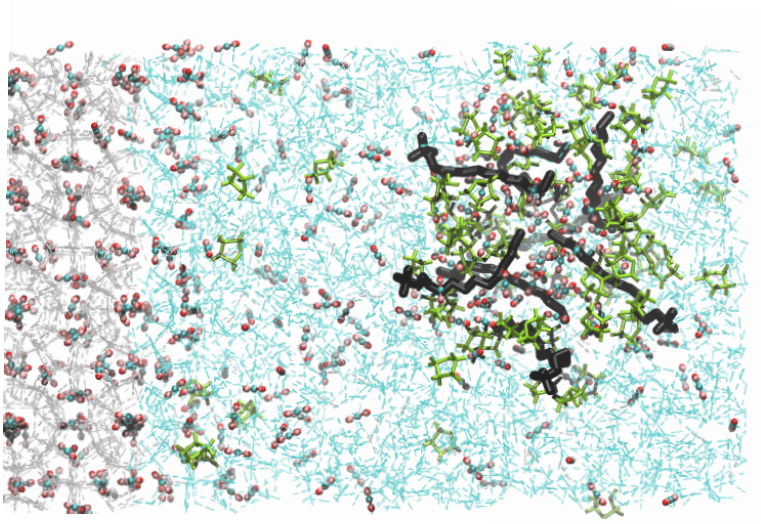

Figure 7: VMD snapshot of SDS aggregates at T = 284.1K where the black molecules are SDS molecules

To understand why SDS aggregates in the simulated system yield structures that differ from the micelles typically observed in liquid water, we conducted a systematic study in which temperature and composition were changed.

Temperature	0 THF	50 THF	100 THF
269.1K	No micelle	No micelle	No micelle
274.1K	No micelle	No micelle	Micelle
279.1K	No micelle	Micelle	Micelle
284.1K	No micelle	Micelle	Micelle

Table 2: Summary of SDS aggregates formation under different temperatures and THF concentrations

As seen in Table 2, we did not observe any aggregation in the systems with no THF, even at the highest temperature considered. The aggregate phase transition temperature increased when the number of THF molecules added to the system was halved. Such observation implies that THF reduces the critical micelle concentration (CMC) of SDS. The potential reason for this phenomenon is that THF may become more insoluble as temperature increases due to the closed-loop miscibility gap within the THF-water binary system [56]. As such, the insolubility of THF in water at the simulation temperature creates an entropic driving force that induces the formation of micelle-like aggregates [57]. Prior studies also established that the CMC of SDS surfactants decreases linearly with a higher concentration of ethers [58], further reinforcing our hypothesis.

Figure 8 shows the number of THF molecules trapped within the SDS aggregates over the entire trajectory at 274.1K (smallest aggregate) and 284.1K (largest aggregate). The results are obtained using the clustering algorithm described in the Methods section. The number of molecules adsorbed increases initially and reaches a constant value when the aggregate is saturated, which is in line with typical micellar behaviour. Noticeably, the aggregates trapped more THF molecules at higher temperatures.

At a similar pressure and concentration used in our set-up, THF will become insoluble between T = 368 K to 404 K [59], which is warmer than the temperature within our

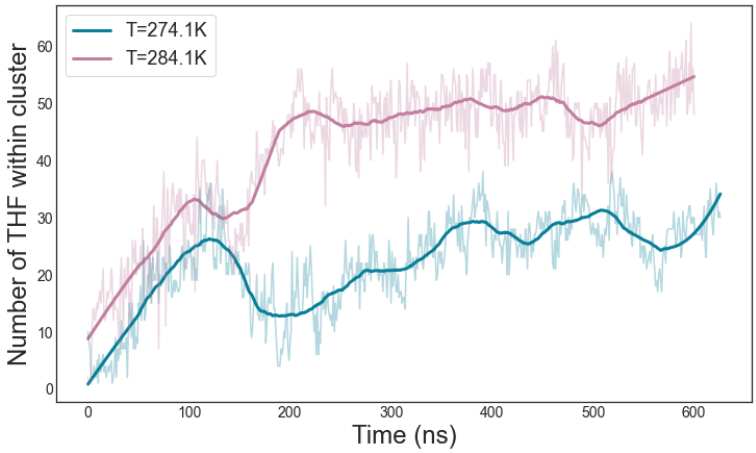

Figure 8: The amount of THF trapped within the SDS aggregates over time in the simulated system containing 100 THF

system. However, the miscibility behaviour of THF in water is highly sensitive to contamination, and the presence of CO_2 and SDS may alter the miscibility curve[56].

3.3. Aggregates Effects on Hydrates Growth

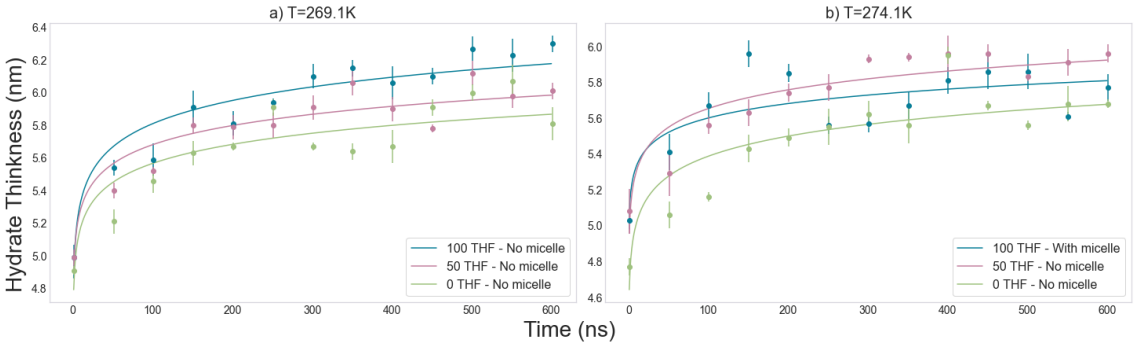

Figure 9: Comparison of hydrate thickness evolution over time when 0/50/100 THF molecules in the system at a) T=269.1K and b) T=274.1K.

The effect of the SDS aggregates on the growth of hydrates can be deduced from Figure 9. At T=269.1K (Figure 9(a)), where no SDS aggregate is formed in any of the three systems, the hydrates have a higher growth rate with increasing THF concentration. Similar phenomena are also observed at T=279.1K, where systems with THF form SDS aggregates and agree well with previous studies by Phan et al. [17]. However, at T=274.1K, the aggregate is formed only in the system with 100 THF. The hydrate growth profile in this system (Figure 9(b)) shows a slower hydrate growth rate than the system without SDS aggregate, despite having more THF. This implies that the SDS micellar aggregate impedes hydrate growth.

Though SDS is generally regarded as a kinetic promoter for gas hydrates, several studies reported that increasing SDS concentration beyond certain limit compromises hydrates growth [18, 60]. Experiments showed that the promotion effect of SDS drops beyond its CMC [61]. Although our observations are obtained at very low SDS concentrations (0.11mol%), it should, however, be remembered that the time scale accessible to atomistic MD simulations is on the order of hundreds of nanoseconds, while the typical exchange rate between surfactants in the bulk and those adsorbed at interfaces or within micelles is of the order of microseconds. To overcome these

differences in time scale, the few SDS molecules present in our system are initially placed on the solid-liquid interface (see Figure 1). Nevertheless, the simulation and the experimental results just summarised are indeed in qualitative agreement.

To identify the molecular mechanism responsible for the observations, we hypothesise a kinetic or thermodynamic effect. In the next paragraphs, we discriminate between the two possibilities.

3.3.1. Hypothesis 1: Kinetic Effects

Lv et al. [60] identified an optimal concentration of surfactant promoters concerning the growth of methane hydrates. Adding beyond the optimal amount leads to a decrease in hydrate growth rate and gas storage capacity. They hypothesised that such phenomena can be ascribed to micelles forming cages that will trap the gas molecules, hindering mass transfer from the liquid to the hydrate. Stimulated by this hypothesis, we delved further into understanding micelles' kinetic and thermodynamic influences on hydrate growth.

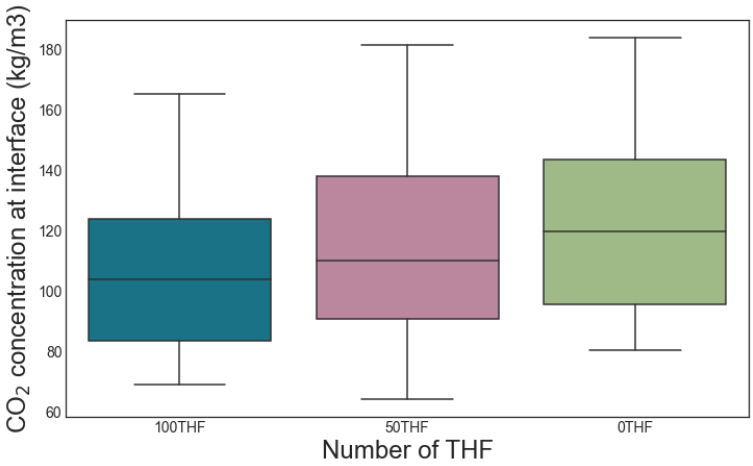

Figure 10: Distribution of CO_2 concentration at the hydrate-liquid interface at T=284.1K

If the SDS aggregates reduce the kinetics of hydrate growth by removing CO_2 from the system, it is plausible that the aggregation would lead to a decrease in the concentration of CO_2 at the interface, which is the rate-limiting step for hydrate growth [62]. Since we observe the presence of SDS aggregation in our systems alongside CO_2, it is reasonable to assume that these aggregates have an impact on the concentration of CO_2 at the interface. Hence, the concentration of CO_2 at the hydrate-liquid interface is analysed at T=284.1K, at which conditions our simulations identify the largest SDS aggregate. The results are illustrated in Figure 10. We acquired interfacial concentrations by identifying the interface using the F4 order parameter and calculated the concentration within the interfacial region (≈1nm thick). It can be inferred from the graph that there are fewer CO_2 molecules at the interface when the SDS aggregate is present (when THF is present), which agrees with the mass transfer limitation hypothesis by Lv and colleagues [60]. However, statistical analysis reveals a different conclusion. We conducted a two-sided t-test between the 100 THF system (which has the largest SDS aggregate) and the 0 THF system using Python's scipy library. The p-value obtained is 0.076, which is slightly higher than 0.05, suggesting that the difference in CO_2 concentration at the interface is not statistically significant. As such, though it is possible that mass transfer limitation could be a factor in the observed behaviour, this hypothesis cannot be conclusively verified.

3.3.2. Hypothesis 2: Thermodynamic Effects

Because the aggregates adsorb and trap a significant amount of THF and CO_2 molecules, impacts could be exerted on hydrate growth. First, trapping the THF molecules will reduce their promoting capability. Second, trapping CO_2 will reduce supersaturation and hence the driving force for hydrate growth.

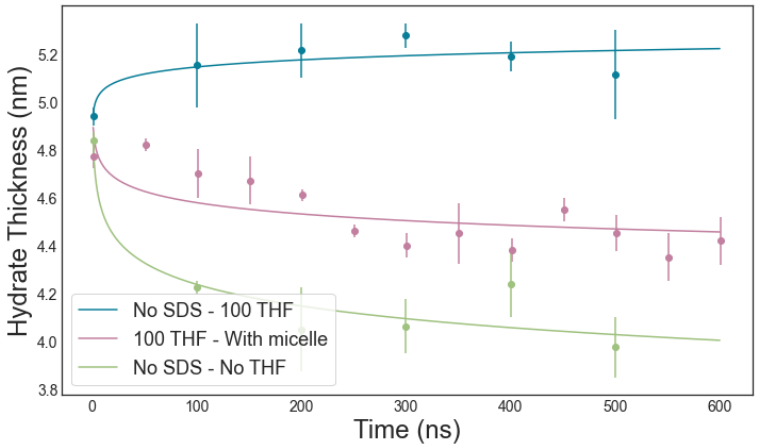

Figure 11: Comparison of hydrate growth removing SDS and CO_2 within SDS aggregates with literature value with no SDS at T=284.1K [17]

Figure 11 demonstrates the difference in hydrate growth between our systems and the results reported by Phan et al. [17]. Their work employed an identical simulation framework to the one considered here, except no SDS was present. Hence, no aggregate formed in the systems studied by Phan et al. We obtained the hydrate thickness data from two of their systems: one with 100 THF and one without at T=284.1 K. Our THF and CO_2 concentration and simulation conditions are also identical. Their results indicated that THF shifts the equilibrium curve to milder conditions, as the hydrates with THF promoters (blue) did not dissociate as much as those with no THF (green). Our system with 100 THF and SDS at T=284.1K lies in between the other two datasets. It is, therefore, apparent that the SDS molecules behave like thermodynamic inhibitors. Figure 8 shows that approximately 50 to 60 THF molecules are trapped within the SDS aggregate. As such, Figure 11 can be viewed as the hydrate growth comparison between systems with 100 THF, 50 THF and 0 THF. The trend illustrated in Figure 11 agrees well with our simulation results at T=269.1K and T=279.1K, where more THF leads to faster growth, as shown in Figure 5. This observation supports the hypothesis that SDS aggregate traps THF molecules, removing them from the hydrate-liquid interface. This mechanism could only partially explain the slower hydrate growth rate obtained for the system with 100 THF compared to 50 THF at T=274.1K, as illustrated in Figure 9 (b). The SDS aggregate in the 100 THF system only traps 20-30 THF molecules, which means there are still more free THF in this system than in the one built to contain 50 THF molecules. This leads us to the second thermodynamic hypothesis: that the aggregates reduce the driving force by sequestering CO_2 molecules.

To test this possibility, we conducted another simulation to understand the significance of reduced CO_2 concentration in the bulk liquid on hydrate growth. We used the same conditions and configurations as the 100 THF system at T=274.1K, but we removed the CO_2 and THF content trapped in the aggregate. To prevent SDS from aggregating, we reduced the hydrocarbon tail to only 5 carbon chains so as to increase

its CMC. Though this would cause a slight deviation in chemical properties from SDS, the change in tail length has a limited impact on hydrate growth at a concentration above 0.1wt% [63], which is significantly lower than the concentration of SDS used in the simulation. The growth profile is presented in Figure 12. It can be deduced from the graph in Figure 12 that reducing CO_2 concentration slows down hydrate growth. However, the data sets are within statistical uncertainty from each other, suggesting that reducing CO_2 concentration is not the only mechanism by which the aggregates affect hydrates growth.

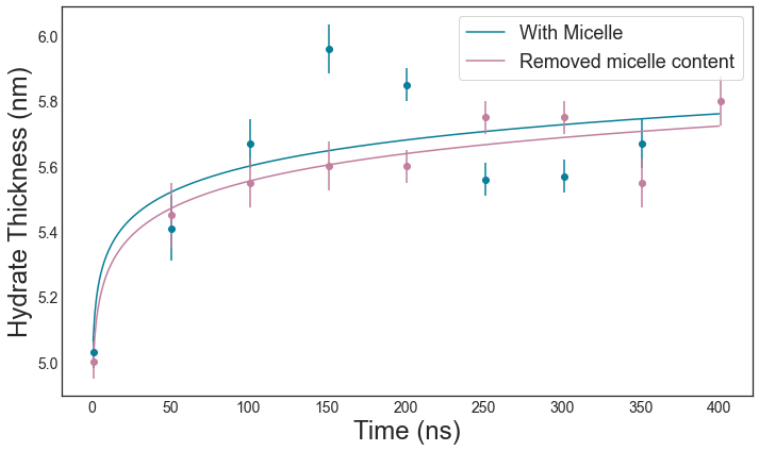

Figure 12: Comparison of hydrate growth removing SDS and CO_2 within SDS aggregates with literature value with no SDS at T=284.1K

4. Experimental Validation

The simulation studies discussed above reveal two significant observations. Firstly, it is observed that THF decreases the critical micelle concentration (CMC) of SDS. Secondly, it is ascertained that the occurrence of such SDS micellar aggregates adversely affects the growth of hydrates. These conclusions were validated using experiments to authenticate their accuracy and robustness.

4.1. Interfacial Tension Measurements

The CMC for each series was determined from the intersection of the concentration-dependent section of the surface tension (ST) graph with the horizontal (concentration-independent) section of the graph. Below the CMC, ST is linearly dependent on the log of concentration, whereby an increase in concentration leads to a concurrent decrease in ST. Such a relationship occurs because the surfactant adsorbs to the droplet's water-air interface and creates a surfactant monolayer. Eventually, at the CMC, the interface is saturated with surfactant molecules and the minimum ST for that surfactant system is reached. Above the CMC, additional surfactant adsorption to this interface is deterred by the established adsorption layer, and surfactant molecules associate into micelles in solution, resulting in little to no further change in ST.

The CMC can be interpolated by fitting lines through the concentration-dependent and independent regions, respectively and determining the intercept of the two lines. In the case of pure SDS, as shown in Figure 13 (a), a CMC value of 7.93 mM was extracted, which is consistent with literature values of 8-8.25 mM at 298K [64, 65].

When THF was added to the SDS-CO_2 solutions, as shown in Figure 13 (b), the measured CMC decreased by 22.2% to 6.17 mM at 298K and atmospheric pressure.

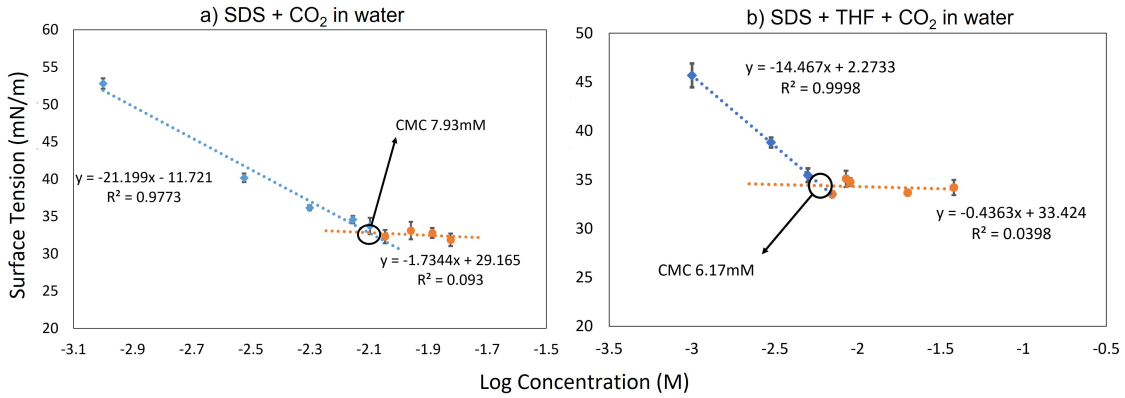

Figure 13: Surface Tension vs log concentration for a) pure SDS solutions in CO_2 saturated water from 0.001M to 0.015M SDS with CMC determined as 7.93mM SDS, and b) THF-SDS solutions in CO_2 saturated water from 0.001M to 0.038M SDS with 0.476M THF with CMC determined as 6.17mM SDS. CMC is calculated by equating the fit lines and solving for the point of intersection. Error bars represent 1 standard deviation and are calculated from three repeat experiments per solution across an average of 10 points per repeat.

The decrease in CMC with both promoters present indicates that the THF and SDS interact in solution and that this interaction causes a decrease in the amount of SDS that can adsorb to the hydrate surface. Such a significant decrease in CMC also reaffirmed simulation observation.

4.2. HP-DSC Results for CO_2 Hydrate Conversion

The effect of promoters (THF, SDS, and the combination of both of them) on CO_2 hydrates properties was inferred by quantities measured during our High-Pressure DSC experiments, such as the percentage of CO_2 hydrate conversion, onset temperatures, and heat released during CO_2 hydrate formation and dissociation.

Pure CO_2 hydrates were first used in our experiments to establish a baseline heat release and conversion. The pure CO_2 hydrate experiment produced a single peak with an average dissociation onset temperature of 6.29 $\pm$ 0.11°C and heat of dissociation of 124.36 $\pm$ 1.53 J/g as produced in Figure **??** (A). This onset temperature is similar to what was obtained by Anderson [50], thereby substantiating the accuracy and validity of our experimental set-up.

Hydrate conversion was compared between CO_2 with SDS at concentrations below and above the CMC, respectively. CO_2-0.001M SDS experiments (below the CMC) produced an average dissociation onset temperature of 6.39 $\pm$ 0.11°C, similar to the pure CO_2 system. This implies that SDS did not affect the thermodynamics of the system. As seen from Figure 14 (B), only a single peak was obtained from the DSC profile, indicating a CO_2 hydrate phase with increased conversion due to the kinetic promotion. CO_2-0.038M SDS (above the CMC) experiments showed a similar DSC profile, with a single peak and an average dissociation onset temperature of 6.38 $\pm$ 0.10°C. The hydrate conversion percentages below and above the CMC are 27 $\pm$ 1.97% and 26 $\pm$ 2.07%, respectively, with no significant difference as shown in Figure 15. These results indicate that, with SDS alone present in the system, the presence of SDS micelles does not affect the performance of the kinetic promoter towards sI CO_2 hydrate. Such observation is consistent with simulation results shown in Figure 10, according to which the kinetic hindrance and reduction of concentration driving force of the micelles are insignificant.

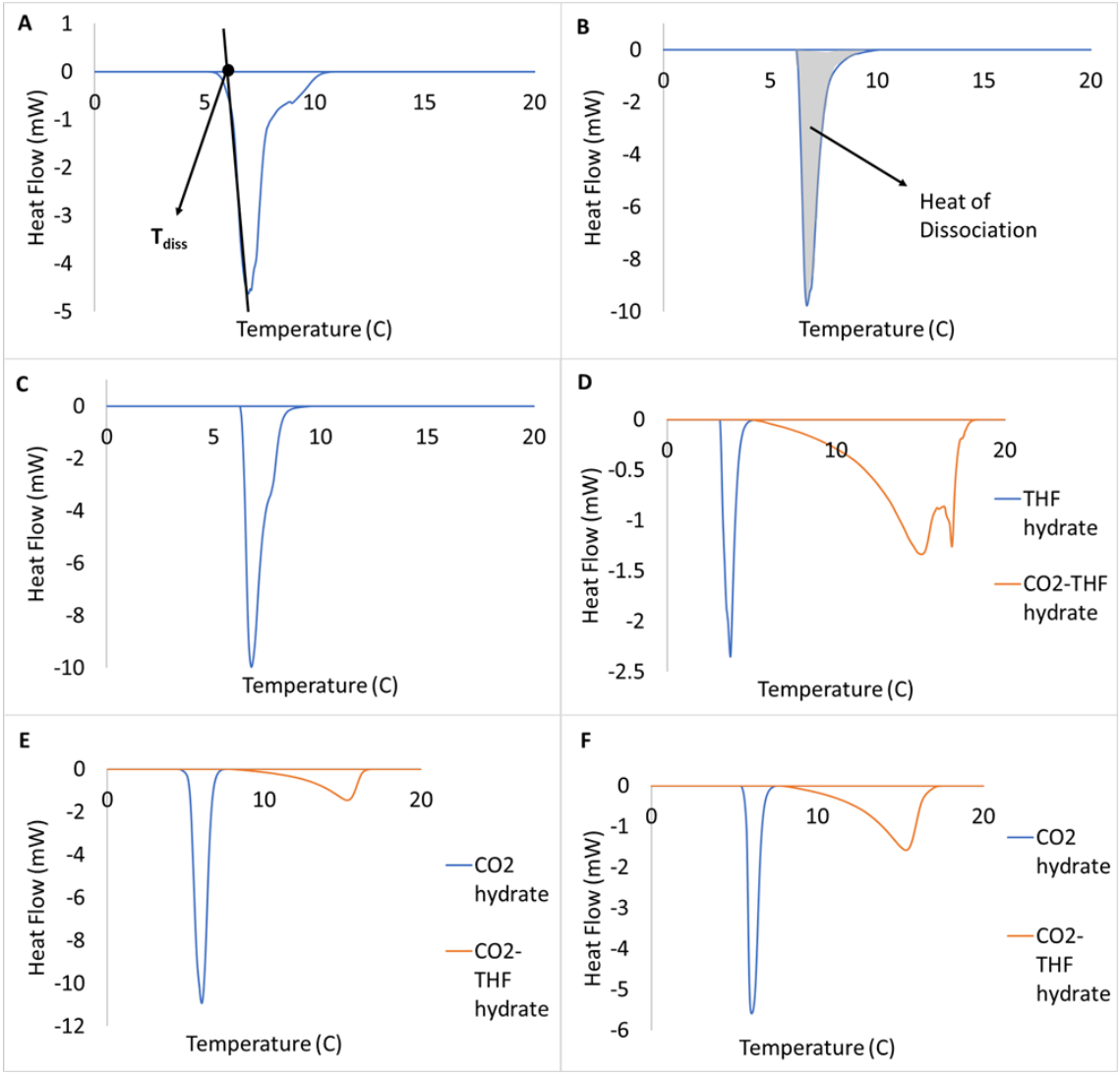

Figure 14: DSC heat flow curves for CO2 and CO2-additive experiments. A: Pure CO2, B: CO2-0.001M SDS below CMC, C: CO2-0.038M SDS above CMC, D: CO2-10wt% THF, E: CO2-10wt% THF- 0.001M SDS below CMC, F: CO2-10wt% THF- 0.038M SDS above CMC. Peaks averaged over 3 repeat experiments for each system tested. results

Next, 10wt% THF was added to the CO_2 hydrate system to determine the effect of THF alone. The DSC profile shown in Figure 14 (D) revealed two distinct peaks corresponding to the formation of THF hydrate and THF-CO_2 hydrate, respectively. The blue curve plotted in Figure 14 D is more likely to be THF hydrates as the onset temperature is 3.38 $\pm$ 0.21°C, which is closer to that of a THF hydrate rather than CO_2 hydrate [29]. The presence of multiple peaks suggests that the addition of THF can cause the formation of mixed hydrate phases, as shown in other works [51, 66, 67, 68]. The THF-CO_2 hydrate (highlighted in orange in Figure 14 D) has a higher dissociation onset temperature of 12.63 $\pm$ 0.82°C as compared to CO_2 and CO_2+SDS systems shown earlier. The temperature shift conforms to the current understanding of THF's thermodynamic promoter role. The broad peak with multiple maxima indicates that there may be CO_2-THF hydrates of different THF composition formed and dissociated during the experiment, which aligns with previous studies [51, 66]. The conversion for the THF hydrate phase was not calculated as it likely did not contain CO_2 [51, 66] and thus would not factor into the total CO_2 conversion. As such, the CO_2 hydrate conversion was computed to be 36 $\pm$ 0.61%.

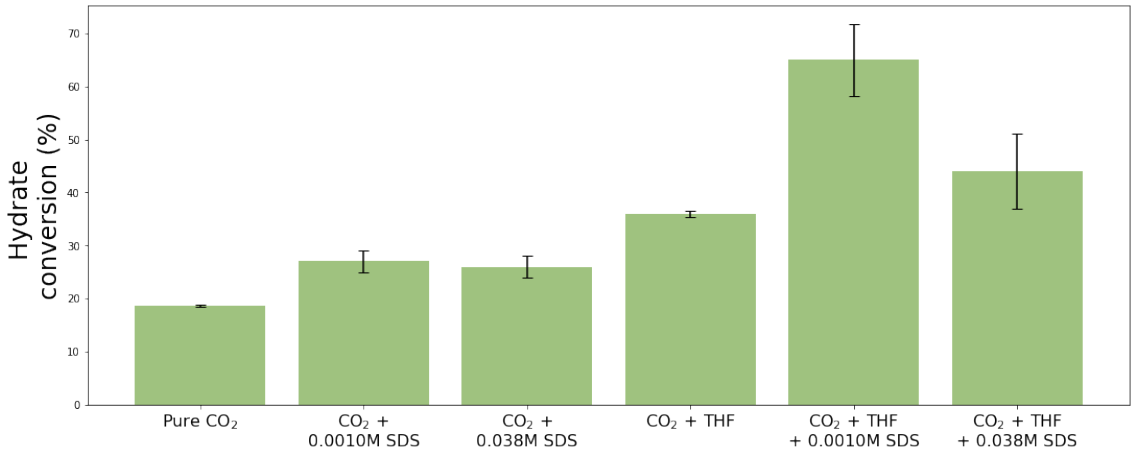

Figure 15: Conversion determined from DSC experiments for CO_2 containing hydrate phases. The experiments were repeated in triplicates to ensure repeatability and reliability of the results

THF-SDS mixtures were tested to determine the effect of the combined promoter system. At both SDS concentrations with THF present, two distinct peaks appeared, indicating hydrates of different compositions may have formed due to THF. The larger, narrow peaks (highlighted in blue) shifted well above the THF hydrate equilibrium temperature and towards the CO_2 hydrate equilibrium temperature, indicating that a pure CO_2 hydrate phase formed in place of the pure THF hydrate phase. The SDS in the system appears to have encouraged the growth of a pure sI CO_2 hydrate phase which did not exist when THF alone was present. This is the same conclusion drawn for methane hydrates by Kumar and colleagues [67]. In both systems, as both hydrates would contain CO_2, the conversion was calculated by adding the individual conversions for the CO_2 and CO_2-THF hydrate. At 0.001M SDS, below the CMC (Figure 14 E), the total conversion is 65 $\pm$ 6.76%. At 0.038M SDS above the CMC (Figure 14 F), the amount of CO_2 hydrate formed decreased, indicated by the lower average heat of dissociation of 83.84 $\pm$ 46.56 J/g at 5.73 $\pm$ 0.09°C, while the CO_2-THF hydrate peak remained almost unchanged. The total CO_2 conversion in this system is computed to be 44 $\pm$ 7.09%.

The comparison of CO_2 conversion in all systems is presented in Figure 15. The results first reaffirmed the discovery that a combination of THF and SDS is better when a single promoter is used. However, more importantly, while SDS added in addition to THF can increase CO_2 hydrate formation, the presence of SDS above its CMC detrimentally impacts the overall growth and conversion of the hydrate, as shown from the lower conversion. Below the CMC, the combined application of SDS and THF drastically increases conversion compared to SDS or THF alone; however, above the CMC, the SDS and THF detrimentally interact, and the total conversion decreases.

5. Conclusions

5.1. Key findings

The synergism vs antagonism between THF and SDS on CO_2 hydrates was investigated using atomistic MD simulation conducted within various temperatures and system compositions. The results show that hydrates grow faster with more THF at T=269.1K and T=279.1K at 25.5 bar. Increasing the temperature to 274.1K and beyond, SDS micellar aggregates could appear, likely due to the increasing entropic

driving force [57]. Lowering THF concentration can prevent the formation of SDS aggregates, which indicates that THF lowers the CMC of SDS. This is confirmed by results obtained from IFT experiments. Simulation results reveal that at T = 284.1K with 100 THF molecules, the hydrates dissociated when SDS micelles existed but grew when no SDS was present at the same conditions. The HP-DSC experiments also indicate a decrease in the dissociation temperature when both THF and SDS are present.

5.2. Key improvements compared to findings in literature

The synergistic influence of THF and SDS on CO_2 hydrates has been extensively observed through various experimental investigations [13, 23]. It has been observed that the addition of an excessive amount of promoters can have a detrimental effect on their overall performance [24, 69]. The present research findings shed light on the existence of an optimal surfactant concentration that is associated with promoting efficient hydrate growth.

5.3. Highlight of hypothesis, new concepts and innovations

The simulation and experiment results indicate that the SDS aggregates behave like thermodynamic inhibitors as they trap THF molecules, essentially removing them and the SDS themselves from the system. Removing THF reduces its thermodynamic stabilisation ability. This phenomenon explains the presence of optimal surfactant concentration related to promoting hydrate growth. CO_2 conversion results obtained from DSC experiments also reinforced this hypothesis. In addition to being consistent with the simulation results, the experiments also show that the CO_2 uptake in hydrates strongly depends on the synergism among the two promoters, with the best results obtained here showing 21% to 46% increase in CO_2 uptake compared to systems without promoters, as well as with system with a sub-optimal composition of the promoters cocktail.

5.4. Vision for future work

These results provide insights into understanding the microscopic behaviours of promoters on hydrate growth and how promoters can interact synergistically and/or antagonistically depending on their relative concentrations and the system conditions.

6. Acknowledgements

Xinrui Cai would like to express her gratitude towards the A&BK studentship that sponsored this project. Alberto Striolo is grateful to the Asahi Chair in Chemical Engineering at the University of Oklahoma, as well as to the EPSRC grant number EP/T004282/1 for financial support. Matteo Salvalaglio acknowledges funding from the Crystallization in the Real World EPSRC Programme Grant (Grant EP/R018820/1) and the EPSRC Frontier Guarantee Grant (EP/X033139/1). Joshua Worley and Carolyn Koh acknowledge funding from the NSF under the CBET grant 2015201 for experimental work. The authors gratefully acknowledge the Archer2 and UCL myriad teams for providing access to their supercomputing facilities and technical support, which have greatly advanced this research project.

References

[1] B. A. Buffett, "Clathrate Hydrates," *Annual Review of Earth and Planetary Sciences*, vol. 28, pp. 477–507, may 2000.

[2] E. D. Sloan Jr. and C. A. Koh, *Clathrate Hydrates of Natural Gases*. CRC Press, 3rd ed., sep 2007.

[3] E. D. Sloan, "Fundamental principles and applications of natural gas hydrates," *Nature*, vol. 426, no. 6964, pp. 353–359, 2003.

[4] H. P. Veluswamy and P. Linga, "Macroscopic kinetics of hydrate formation of mixed hydrates of hydrogen/tetrahydrofuran for hydrogen storage," *International Journal of Hydrogen Energy*, vol. 38, pp. 4587–4596, apr 2013.

[5] H. J. Lee, J. D. Lee, P. Linga, P. Englezos, Y. S. Kim, M. S. Lee, and Y. D. Kim, "Gas hydrate formation process for pre-combustion capture of carbon dioxide," *Energy*, vol. 35, no. 6, pp. 2729–2733, 2010.

[6] M. Yang, H. Zhou, P. Wang, N. Li, and Y. Song, "Hydrate-based CO2 capture from flue gas in constant pressure process with the presence of THF," *Energy Procedia*, vol. 142, pp. 3939–3943, 2017.

[7] S. Lee, L. Liang, D. Riestenberg, O. R. West, C. Tsouris, and E. Adams, "CO 2 Hydrate Composite for Ocean Carbon Sequestration," *Environmental Science & Technology*, vol. 37, pp. 3701–3708, aug 2003.

[8] T. Saikia and A. Sultan, "Hydrate-based CO2 separation," in *Emerging Carbon Capture Technologies*, ch. 7, pp. 193–237, Elsevier Inc., 2022.

[9] P. W. Wang, D. T. Wu, and S. T. Lin, "Promotion mechanism for the growth of CO2hydrate with urea using molecular dynamics simulations," *Chemical Communications*, vol. 57, no. 43, pp. 5330–5333, 2021.

[10] H. Dashti, L. Zhehao Yew, and X. Lou, "Recent advances in gas hydrate-based CO2 capture," *Journal of Natural Gas Science and Engineering*, vol. 23, pp. 195–207, 2015.

[11] A. A. Majid, J. Worley, and C. A. Koh, "Thermodynamic and Kinetic Promoters for Gas Hydrate Technological Applications," *Energy and Fuels*, vol. 35, no. 23, pp. 19288–19301, 2021.

[12] Y. Li, A. M. Gambelli, F. Rossi, and S. Mei, "Effect of promoters on CO2 hydrate formation: thermodynamic assessment and microscale Raman spectroscopy/hydrate crystal morphology characterization analysis," *Fluid Phase Equilibria*, vol. 550, p. 113218, 2021.

[13] H. P. Veluswamy, K. P. Premasinghe, and P. Linga, "CO2 Hydrates - Effect of Additives and Operating Conditions on the Morphology and Hydrate Growth," *Energy Procedia*, vol. 105, pp. 5048–5054, 2017.

[14] N. Xu, Y. Liu, Z. Cheng, S. Wang, L. Jiang, and Y. Song, "Morphology-Based Kinetic Study of the Formation of Carbon Dioxide Hydrates with Promoters," *Energy & Fuels*, vol. 34, pp. 7307–7315, jun 2020.

[15] O. Salako, C. Lo, J. Zhang, A. Couzis, P. Somasundaran, and J. Lee, "Adsorption of sodium dodecyl sulfate onto clathrate hydrates in the presence of salt," *Journal of Colloid and Interface Science*, vol. 386, pp. 333–337, nov 2012.

[16] S. P. Kang, H. Lee, C. S. Lee, and W. M. Sung, "Hydrate phase equilibria of the guest mixtures containing CO2, N2 and tetrahydrofuran," *Fluid Phase Equilibria*, vol. 185, no. 1-2, pp. 101–109, 2001.

[17] A. Phan, H. Schlösser, and A. Striolo, "Molecular mechanisms by which tetrahydrofuran affects CO2 hydrate Growth: Implications for carbon storage," *Chemical Engineering Journal*, vol. 418, no. December 2020, pp. 34–37, 2021.

[18] L. Liu, Y. Yao, X. Zhou, Y. Zhang, and D. Liang, "Improved formation kinetics of carbon dioxide hydrate in brine induced by sodium dodecyl sulfate," *Energies*, vol. 14, no. 8, 2021.

[19] D. L. Zhong, S. Y. He, D. J. Sun, and C. Yang, "Comparison of methane hydrate formation in stirred reactor and porous media in the presence of SDS," *Energy Procedia*, vol. 61, pp. 1573–1576, 2014.

[20] N. S. Molokitina, A. N. Nesterov, L. S. Podenko, and A. M. Reshetnikov, "Carbon dioxide hydrate formation with SDS: Further insights into mechanism of gas hydrate growth in the presence of surfactant," *Fuel*, vol. 235, no. March 2018, pp. 1400–1411, 2019.

[21] C. Lo, J. Zhang, P. Somasundaran, and J. W. Lee, "Investigations of surfactant effects on gas hydrate formation via infrared spectroscopy," *Journal of Colloid and Interface Science*, vol. 376, pp. 173–176, jun 2012.

[22] H. Liang, D. Guan, Y. Liu, L. Zhang, J. Zhao, L. Yang, and Y. Song, "Kinetic process of upward gas hydrate growth and water migration on the solid surface," *Journal of Colloid and Interface Science*, vol. 626, pp. 1003–1014, nov 2022.

[23] J. P. Torré, M. Ricaurte, C. Dicharry, and D. Broseta, "CO 2 enclathration in the presence of water-soluble hydrate promoters: Hydrate phase equilibria and kinetic studies in quiescent conditions," *Chemical Engineering Science*, vol. 82, pp. 1–13, 2012.

[24] H. Wang, Q. Wu, and B. Zhang, "Influence of THF and THF/SDS on the Kinetics of CO2 Hydrate Formation Under Stirring," *Frontiers in Energy Research*, vol. 9, feb 2021.

[25] A. Demurov, R. Radhakrishnan, and B. L. Trout, "Computations of diffusivities in ice and CO2 clathrate hydrates via molecular dynamics and Monte Carlo simulations," *The Journal of Chemical Physics*, vol. 116, pp. 702–709, jan 2002.

[26] N. I. Papadimitriou, I. N. Tsimpanogiannis, I. G. Economou, and A. K. Stubos, "Monte Carlo simulations of the separation of a binary gas mixture (CH 4 + CO 2) using hydrates," *Physical Chemistry Chemical Physics*, vol. 20, no. 44, pp. 28026–28038, 2018.

[27] Y. J. Lee, T. Kawamura, Y. Yamamoto, and J. H. Yoon, "Phase equilibrium studies of tetrahydrofuran (THF) + CH4, THF + CO2, CH4 + CO2, and THF + CO2 + CH4 hydrates," *Journal of Chemical and Engineering Data*, vol. 57, no. 12, pp. 3543–3548, 2012.

[28] F. Takeuchi, M. Hiratsuka, R. Ohmura, S. Alavi, A. K. Sum, and K. Yasuoka, "Water proton configurations in structures I, II, and H clathrate hydrate unit cells," *Journal of Chemical Physics*, vol. 138, no. 12, 2013.

[29] A. Delahaye, L. Fournaison, S. Marinhas, I. Chatti, J.-P. Petitet, D. Dalmazzone, and W. Fürst, "Effect of THF on Equilibrium Pressure and Dissociation Enthalpy of CO 2 Hydrates Applied to Secondary Refrigeration," *Industrial Engineering Chemistry Research*, vol. 45, pp. 391–397, jan 2006.

[30] L. Jensen, K. Thomsen, N. von Solms, S. Wierzchowski, M. R. Walsh, C. A. Koh, E. D. Sloan, D. T. Wu, and A. K. Sum, "Calculation of Liquid Water-Hydrate-Methane Vapor Phase Equilibria from Molecular Simulations," *The Journal of Physical Chemistry B*, vol. 114, pp. 5775–5782, may 2010.

[31] J. M. Míguez, M. M. Conde, J. P. Torré, F. J. Blas, M. M. Piñeiro, and C. Vega, "Molecular dynamics simulation of CO2 hydrates: Prediction of three phase coexistence line," *Journal of Chemical Physics*, vol. 142, no. 12, 2015.

[32] M. M. Conde and C. Vega, "Determining the three-phase coexistence line in methane hydrates using computer simulations," *The Journal of Chemical Physics*, vol. 133, p. 064507, aug 2010.

[33] J. G. Harris and K. H. Yung, "Carbon Dioxide's Liquid-Vapor Coexistence Curve And Critical Properties as Predicted by a Simple Molecular Model," *The Journal of Physical Chemistry*, vol. 99, pp. 12021–12024, aug 1995.

[34] Y. T. Tung, L. J. Chen, Y. P. Chen, and S. T. Lin, "Growth of structure i carbon dioxide hydrate from molecular dynamics simulations," *Journal of Physical Chemistry C*, vol. 115, no. 15, pp. 7504–7515, 2011.

[35] P. Procacci, "PrimaDORAC: A Free Web Interface for the Assignment of Partial Charges, Chemical Topology, and Bonded Parameters in Organic or Drug Molecules," *Journal of Chemical Information and Modeling*, vol. 57, pp. 1240–1245, jun 2017.

[36] H. Dominguez and M. L. Berkowitz, "Computer Simulations of Sodium Dodecyl Sulfate at Liquid/Liquid and Liquid/Vapor Interfaces," *The Journal of Physical Chemistry B*, vol. 104, pp. 5302–5308, jun 2000.

[37] V. K. Michalis, I. N. Tsimpanogiannis, A. K. Stubos, and I. G. Economou, "Direct phase coexistence molecular dynamics study of the phase equilibria of the ternary methane-carbon dioxide-water hydrate system," *Physical Chemistry Chemical Physics*, vol. 18, no. 34, pp. 23538–23548, 2016.

[38] H. Berendsen, D. van der Spoel, and R. van Drunen, "GROMACS: A message-passing parallel molecular dynamics implementation," *Computer Physics Communications*, vol. 91, pp. 43–56, sep 1995.

[39] H. J. C. Berendsen, J. P. M. Postma, W. F. van Gunsteren, A. DiNola, and J. R. Haak, "Molecular dynamics with coupling to an external bath," *The Journal of Chemical Physics*, vol. 81, pp. 3684–3690, oct 1984.

[40] D. J. Evans and B. L. Holian, "The Nose–Hoover thermostat," *The Journal of Chemical Physics*, vol. 83, pp. 4069–4074, oct 1985.

[41] M. Parrinello and A. Rahman, "Crystal Structure and Pair Potentials: A Molecular-Dynamics Study," *Physical Review Letters*, vol. 45, pp. 1196–1199, oct 1980.

[42] T. Yagasaki, M. Matsumoto, and H. Tanaka, "Mechanism of Slow Crystal Growth of Tetrahydrofuran Clathrate Hydrate," *The Journal of Physical Chemistry C*, vol. 120, pp. 3305–3313, feb 2016.

[43] S. Adisasmito, R. J. Frank, and E. D. Sloan, "Hydrates of carbon dioxide and methane mixtures," *Journal of Chemical & Engineering Data*, vol. 36, pp. 68–71, jan 1991.

[44] P. Rodger, T. Forester, and W. Smith, "Simulations of the methane hydrate/methane gas interface near hydrate forming conditions conditions," *Fluid Phase Equilibria*, vol. 116, pp. 326–332, mar 1996.

[45] T. Bui, F. Sicard, D. Monteiro, Q. Lan, M. Ceglio, C. Burress, and A. Striolo, "Antiagglomerants Affect Gas Hydrate Growth," *Journal of Physical Chemistry Letters*, vol. 9, no. 12, pp. 3491–3496, 2018.

[46] K. W. Hall, S. Carpendale, and P. G. Kusalik, "Evidence from mixed hydrate nucleation for a funnel model of crystallization," 2016.

[47] G. A. Tribello, F. Giberti, G. C. Sosso, M. Salvalaglio, and M. Parrinello, "Analyzing and driving cluster formation in atomistic simulations," *Journal of chemical theory and computation*, vol. 13, no. 3, pp. 1317–1327, 2017.

[48] L. Kollias, R. Rousseau, V.-A. Glezakou, and M. Salvalaglio, "Understanding metal–organic framework nucleation from a solution with evolving graphs," *Journal of the American Chemical Society*, vol. 144, no. 25, pp. 11099–11109, 2022.

[49] S. Denning, A. A. Majid, J. M. Lucero, J. M. Crawford, M. A. Carreon, and C. A. Koh, "Metal–Organic Framework HKUST-1 Promotes Methane Hydrate Formation for Improved Gas Storage Capacity," *ACS Applied Materials Interfaces*, vol. 12, pp. 53510–53518, nov 2020.

[50] G. K. Anderson, "Enthalpy of dissociation and hydration number of carbon dioxide hydrate from the Clapeyron equation," *The Journal of Chemical Thermodynamics*, vol. 35, pp. 1171–1183, jul 2003.

[51] M. C. Martínez, D. Dalmazzone, W. Fürst, A. Delahaye, and L. Fournaison, "Thermodynamic properties of THF + CO2 hydrates in relation with refrigeration applications," *AIChE Journal*, vol. 54, pp. 1088–1095, apr 2008.

[52] Q. Sun and Y. T. Kang, "Review on CO2 hydrate formation/dissociation and its cold energy application," *Renewable and Sustainable Energy Reviews*, vol. 62, pp. 478–494, 2016.

[53] P. Zhang, Q. Wu, C. Mu, and X. Chen, "Nucleation Mechanisms of CO2 Hydrate Reflected by Gas Solubility," *Scientific Reports*, vol. 8, no. 1, pp. 1–12, 2018.

[54] L. S. Chu, D. T. Wu, and S. T. Lin, "Theory and Kinetic Monte Carlo Simulation of Guest Molecule Transport in sI Clathrate Hydrates Based on Cage Hopping," *Journal of Physical Chemistry C*, vol. 123, no. 17, pp. 11233–11243, 2019.

[55] M. Pisárčik, F. Devínsky, and M. Pupák, "Determination of micelle aggregation numbers of alkyltrimethylammonium bromide and sodium dodecyl sulfate surfactants using time-resolved fluorescence quenching," *Open Chemistry*, vol. 13, dec 2015.

[56] M. D. Smith, B. Mostofian, L. Petridis, X. Cheng, and J. C. Smith, "Molecular Driving Forces behind the Tetrahydrofuran-Water Miscibility Gap," *Journal of Physical Chemistry B*, vol. 120, no. 4, pp. 740–747, 2016.

[57] L. Maibaum, A. R. Dinner, and D. Chandler, "Micelle Formation and the Hydrophobic Effect," *The Journal of Physical Chemistry B*, vol. 108, pp. 6778–6781, may 2004.

[58] M. Manabe and M. Koda, "The Effect of Poly(oxyethylene) Alkyl Ethers, Alkanediols, and Alkanols on the Critical Micelle Concentration of Sodium Dodecyl Sulfate," *Bulletin of the Chemical Society of Japan*, vol. 51, no. 6, pp. 1599–1601, 1978.

[59] N. Riesco and J. Trusler, "Novel optical flow cell for measurements of fluid phase behaviour," *Fluid Phase Equilibria*, vol. 228-229, pp. 233–238, feb 2005.

[60] X. Lv, D. Lu, Y. Liu, S. Zhou, J. Zuo, H. Jin, B. Shi, and E. Li, "Study on methane hydrate formation in gas-water systems with a new compound promoter," *RSC Advances*, vol. 9, no. 57, pp. 33506–33518, 2019.

[61] J. Tang, D. Zeng, C. Wang, Y. Chen, L. He, and N. Cai, "Study on the influence of SDS and THF on hydrate-based gas separation performance," *Chemical Engineering Research and Design*, vol. 91, pp. 1777–1782, sep 2013.

[62] A. Phan, M. Stamatakis, C. A. Koh, and A. Striolo, "Microscopic insights on clathrate hydrate growth from non-equilibrium molecular dynamics simulations," *Journal of Colloid and Interface Science*, vol. 649, pp. 185–193, nov 2023.

[63] T. Daimaru, A. Yamasaki, and Y. Yanagisawa, "Effect of surfactant carbon chain length on hydrate formation kinetics," *Journal of Petroleum Science and Engineering*, vol. 56, pp. 89–96, mar 2007.

[64] T. P. Niraula, A. Bhattarai, and S. K. Chatterjee, "Critical micelle concentration of sodium dodecyl sulphate in pure water and in methanol-water mixed solvent media in presence and absence of KCl by surface tension and viscosity methods," *BIBECHANA*, vol. 11, pp. 103–112, may 2014.

[65] Y. Moroi, K. Motomura, and R. Matuura, "The critical micelle concentration of sodium dodecyl sulfate-bivalent metal dodecyl sulfate mixtures in aqueous solutions," *Journal of Colloid and Interface Science*, vol. 46, pp. 111–117, jan 1974.

[66] Q. Sun, S. Kim, and Y. T. Kang, "Study on dissociation characteristics of CO2 hydrate with THF for cooling application," *Applied Energy*, vol. 190, pp. 249–256, mar 2017.

[67] A. Kumar, R. Kumar, and P. Linga, "Sodium Dodecyl Sulfate Preferentially Promotes Enclathration of Methane in Mixed Methane-Tetrahydrofuran Hydrates," *iScience*, vol. 14, pp. 136–146, apr 2019.

[68] A. Kumar, N. Daraboina, R. Kumar, and P. Linga, "Experimental Investigation To Elucidate Why Tetrahydrofuran Rapidly Promotes Methane Hydrate Formation Kinetics: Applicable to Energy Storage," *The Journal of Physical Chemistry C*, vol. 120, pp. 29062–29068, dec 2016.

[69] D. Mech, P. Gupta, and J. S. Sangwai, "Kinetics of methane hydrate formation in an aqueous solution of thermodynamic promoters (THF and TBAB) with and without kinetic promoter (SDS)," *Journal of Natural Gas Science and Engineering*, vol. 35, pp. 1519–1534, sep 2016.